Misfit Dislocation Sources at Surface Ripple Troughs in Continuous Heteroepitaxial Layers

A. G. Cullis, A. J. Pidduck, and M. T. Emeny

Defense Research Agency, St. Anspecdrews Road, Malvern, Worcs WR14 3PS, England

(Received 14 February 1995)

The present work examines ordered surface ripple arrays exhibited by continuous epitaxial InGaAs on GaAs and, for the first time, demonstrates directly that ripple trough locations are sources for misfit defects at the heteroepitaxial interface. Defect nucleation can take place due to the enhanced stress at such troughs. The first stress-relieving defects observed to form are faulted dislocation half-loops on inclined {111} planes.

The growth of heteroepitaxial semiconductor layers is of considerable importance for advanced electronic device technology. However, misfit stress relief by the introduction of interfacial dislocations degrades the quality of the epitaxy, and limits the performance of devices fabricated in the layers. Therefore, for many years a large amount of work has been directed toward the identification of misfit dislocation sources in the layers. Following the derivation [1,2] of the basic misfitting layer energy expressions, the way in which misfit dislocations can enter a layer by the glide of existing threading dislocations was examined [3–6]. Furthermore, in addition to the operation of specific heterogeneous dislocation sources [7,8], it has been found [9,10] that misfit dislocations can be formed by nucleation of half-loops at the overlayer free surface, and the stability of such loop nuclei has been analyzed [11,12]. In general, it is clear [13] that the kinetic barrier to such nucleation at a perfect, flat surface is predicted to be so large that the process is unlikely to commonly occur.

The surfaces of epitaxial layers can exhibit important deviations from planarity under a number of circumstances. Randomly positioned growth nuclei can form, especially for high strain systems, and local strain relaxation at the nucleus location can then take place [14–16]. Furthermore, it has recently been demonstrated that arrays of ordered ripples can be produced [17–21] upon the surfaces of continuous epitaxial layers, especially in systems of large misfit prepared at high growth temperatures [19,20,22]. Such undulations form as a result of energy minimization in the epitaxial system [23], and yield substantial elastic strain relief. The latter is due to lattice relaxation in the ripple crests, as can be directly measured by transmission electron microscope (TEM) imaging [21]. There is a corresponding increase in stress at the ripple troughs which, based upon studies describing dislocation generation in the stress fields of depressions [24], is expected to promote the nucleation of misfit dislocations. A particularly detailed analysis of the increased probability of dislocation nucleation at unstable cusps in the growth surface has been made [25]. However, experimental evidence for the operation of this generic dislocation formation mechanism in epitaxial systems has not been available until this time. It is the purpose of this paper to present the first direct evidence for dislocation nucleation at ripple troughs in continuous epitaxial layers. It is demonstrated for InGaAs epitaxial alloy on GaAs that there is a direct correlation between the positions of the troughs and individual dislocations injected to relieve the misfit stress.

In these investigations, $In_xGa_{1-x}As$ layers were grown by molecular beam epitaxy on (100) GaAs substrates at a growth rate of 1.0 ml s^{-1} which was corrected for any In desorption at growth temperatures employed. Deposition rate and alloy composition were measured from group-III-induced reflection high-energy electron diffraction (RHEED) oscillations immediately prior to growth. The V/III beam equivalent pressure ratio was maintained at 5:1 for the alloy growth. Substrate temperatures were set with reference to the (4×2)-(2×2) RHEED reconstruction change at the substrate surface immediately prior to growth. Each wafer had 200 nm of GaAs grown as a buffer layer, followed by a pause, before continuing with alloy growth. Layers were studied *ex situ* using a JEOL JEM 4000EX TEM operated at an accelerating voltage of 400 kV; specimens were thinned to electron transparency in plan view and cross-sectional configurations using sequential mechanical polishing and Ar^+ ion milling. Atomic force microscope observations were carried out using a Nanoscope III instrument with silicon nitride stylus.

It has been found that, although $In_xGa_{1-x}As$ layers with low x values exhibit excellent planarity at an x value approaching 0.25, a dramatic structure transition occurs to morphologically undulating growth [26,27]. The roughened layers give the opportunity to study details of the role of surface undulations in the misfit dislocation introduction mechanism. It is especially instructive to examine a roughened $In_xGa_{1-x}As$ alloy with the lowest possible x-value (composition close to the transition value) since this maximizes the thickness of continuous undulating layers which may be found in substantially dislocation-free condition. Growth at a relatively high temperature also promotes the formation of well-ordered ripple arrays [20].

Following these considerations, Fig. 1(a) shows a cross-sectional view of an $In_{0.25}Ga_{0.75}As$ layer on GaAs

(mean strain 1.8%), grown at 580 °C, with a mean thickness of 20 nm. It is evident that the layer is continuous and exhibits ripples of amplitude ~20 nm, with crests of ~30 nm and troughs of ~10 nm thickness. The ripple slopes are generally faceted at ~12°–16° (or occasionally higher angles) so that, while the crests are rounded, the troughs often take the form of relatively sharp grooves. This general morphology exhibits many similarities [21] with that of rippled SiGe layers on Si. Examination of a plan-view TEM image [Fig. 1(b)] of the layer just described shows the array of interacting ripples very clearly, the black or white strain contrast being surface slope dependent [19] due to lattice relaxation at the ripple crests and additional compression at the troughs. The surface undulations take the form of an interlocking array of ridges and mounds resulting, in part, from ripple interference, with the angularity of the contrast features being due to the ripple faceting. The ripples, of wavelength ~100 nm, are generally aligned along orthogonal $\langle 001 \rangle$-type directions, as in the case of SiGe alloy layers on Si, although sometimes local $[0\bar{1}1]$ alignment is evident. The variation of TEM ripple contrast with sample tilt [26], interpreted using an Airy stress function analysis by direct analogy with the SiGe case [21], indicates that compressive stresses at the trough minima are several times the basic misfit stress. Therefore, it is anticipated that misfit defect nucleation at these locations would be especially favorable.

Close inspection of Fig. 1(b) indicates that misfit defect segment generation has just begun (typical short segments are arrowed). However, to determine their relationship to the ripple requires careful image contrast analysis in order to unambiguously distinguish peaks from troughs. It

FIG. 1. (a) Cross-sectional [011] TEM image showing profile of surface ripples on $In_{0.25}Ga_{0.75}As$ epitaxial layer on GaAs, and (b) plan-view, strong-beam, $g = 022$, TEM image showing ordered ripple array and misfit defects (arrowed).

is possible to circumvent this problem with the present sample since the layer is at the very edge or morphological stability and, toward the periphery of the wafer, slight temperature depression caused the formation of ordered but discontinuous ripple arrays. At the edges of such arrays, it is then possible to determine the local surface slope unambiguously. Such an area is shown in Fig. 2, which illustrates the initial formation of local domains of ordered ripples with, in this case, dominant $[0\bar{1}1]$ alignment. The manner in which the surface instability fluctuates from region to region is itself interesting, but this will be discussed elsewhere [26]. However, it is most important in the present context that misfit dislocation generation has specific relationship to the periodicity of the remaining ordered ripples.

Figure 2(a) presents an image recorded using a $0\bar{2}2$ g vector: This shows the ripple domains and groups of misfit defect segments, which occur only in rippled areas. Furthermore, the defects occur primarily along only a preferred [011]-type in-plane direction, a previously observed asymmetry [28]. In order to display the segments more clearly, Fig. 2(b) shows a weak-beam image of the same area, such that the ripples are almost out of contrast, while the defect segments are clearly visible (and indicated by arrows). Where the segments are present in pairs, triples, etc., their local spacing is essentially the [011] ripple wavelength of ~120–130 nm. To locate precisely the defects within the ripple undulations, it is necessary to eliminate the contrast interactions between the structures while maintaining the visibility of both. This is achieved in Figs. 2(c) and 2(d) [areas centered on the labeled defects in Fig. 2(b)], which were recorded using a 022 g vector. Although almost all of each defect is out of contrast, the surface terminations of the defects are still visible as contrast points due to strain-field surface relaxation.

In Fig. 2(c), relatively isolated ripple feature 1 and ripple features 2–10 all give bright or dark contrast with inversion boundaries normal to the direction of the g vector of the operating reflection. Careful analysis of the symmetry of the contrast unambiguously demonstrates [29] that all such features are crests (ridges) in the undulating surface. It is immediately evident that the misfit defect segments are almost always present only in the troughs between ripple ridge sections. For example, segment A-A' extends from the upper edge of ridge section 10 (between sections 8 and 9). Segment B-B' extends from the upper edge of ridge section 7 (between sections 4 and 5). Occasionally, dislocation segments can cut across ridges, as in the case of C-C', which extends from the upper edge of ridge section 6 (between sections 3 and 4), underneath 2, and out into a planar region (at C'). The same behavior is exhibited in the layer area of Fig. 2(d). Misfit defect segments D-D', E-E', F-F', G-G', H-H', I-I', and J-J' are present between the ripple ridge sections marked with circles. Thus it is clear that, as predicted [21,25], misfit defect segments nucleate preferentially in the high
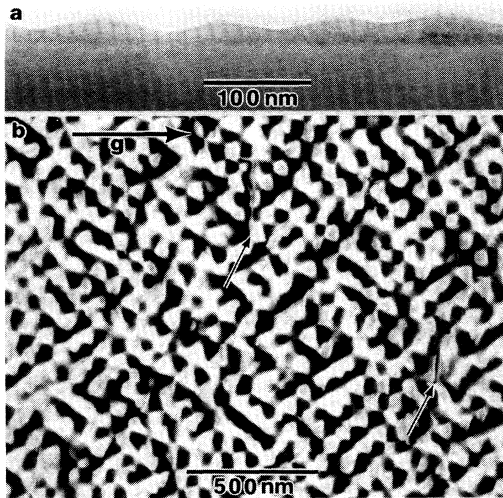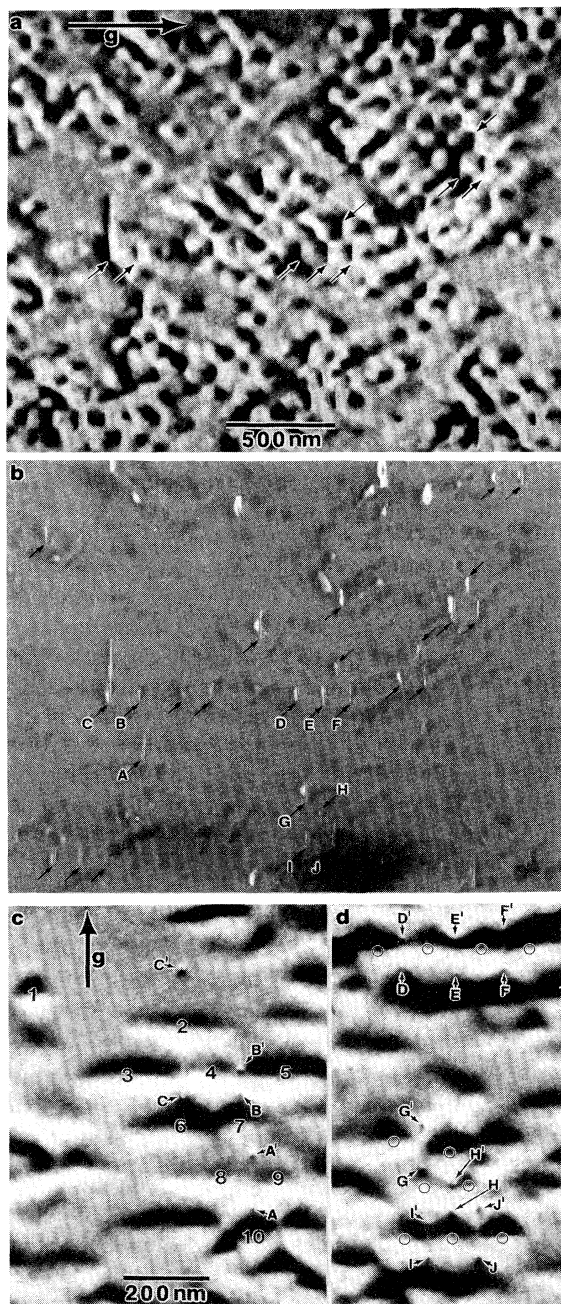
FIG. 2.   Plan-view TEM images showing misfit defects among discontinuous ordered ripple arrays (a) strong-beam, **g** = 0$\bar{2}$2, (Bragg deviation positive) with a selection of misfit defects arrowed; (b) weak-beam, dark-field **g** = 0$\bar{2}$2 with misfit defects arrowed; (c),(d) strong-beam **g** = 022 (Bragg deviation positive) showing misfit defect terminations A-A' to J-J' and selected surface ripple ridge sections numbered in (c) and marked with circles in (d).

stress regions at ripple troughs. In this way, the defect arrangement and spacing conform to the pseudohexagonal symmetry of the ripple arrays.

The invisibility of misfit defects for an operating 022 Bragg reflection indicates that their Burgers (displacement) vectors lie perpendicular to their lengths. However, it has also been found that the defects are in contrast for all 111-type reflections at ~35° to the substrate plane. This indicates that the misfit defects are most likely to be faulted Frank dislocation half-loops with $(a/3)\langle\bar{1}1\bar{1}\rangle$-type Burgers vectors inclined to the foil plane, which is analogous to defect formation in heteroepitaxial metal layers [10]. This deduction has been substantiated by direct high resolution imaging of InGaAs/GaAs cross sections showing the structure of these defects. A typical high resolution lattice image is shown in Fig. 3, where intrinsic stacking fault P extends from near the base of a ripple trough down to Frank partial dislocation Q, which is close to the InGaAs/GaAs interface. Another fault (R) originates in the trough but, in this case, terminates in an $(a/6)\langle 01\bar{1}\rangle$-type stair-rod partial dislocation S, from which additional fault T extends back up to the layer surface. Defects in these cross sections were overwhelmingly present at ripple trough locations.

The work of the present paper shows that, for nucleation of misfit defects in high strain epitaxial systems, intrinsic Frank partial dislocations can be produced first. The mechanism is probably by aggregation of vacancies, which may diffuse in from the layer surface and provide partial local stress relief by the effective removal of material from the compressed region. It is proposed that the observed fault pair formation can then occur by emission of a suitable Shockley partial dislocation on the appropriate intersecting (111)-type plane,

$$(a/3)[\bar{1}1\bar{1}] \rightarrow (a/6)[01\bar{1}] + (a/6)[\bar{2}1\bar{1}].$$

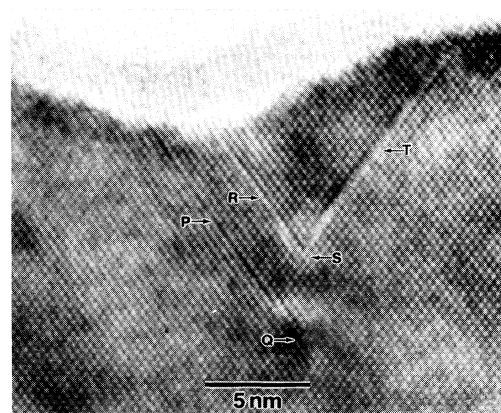Furthermore, it is often stated [28] that the formation

FIG. 3.   Cross-sectional high resolution TEM image, [011] surface normal, showing misfit defects nucleated at surface ripple trough: stacking fault (P) bounded by Frank partial dislocation (Q, note terminating lattice fringe parallel to fault plane) and stacking fault (R) bounded by stair-rod dislocation (S) leading to secondary fault (T).

of edge misfit dislocations of sessile Lomer type (which were seen in thicker, high-strain InGaAs layers) is not understood, but probably involves a climb process. It is now proposed that such Lomer dislocations may be produced by the reaction of an initially formed Frank partial dislocation with a Shockley partial dislocation, which moves in from the surface and annihilates the fault,

$$(a/3)[\bar{1}1\bar{1}] \rightarrow (a/6)[21\bar{1}] + (a/2)[01\bar{1}].$$
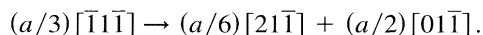
This formation mechanism accounts for the occurrence of sessile Lomer dislocations well beneath the surface of an epitaxial layer.

In summary, the present work has demonstrated experimentally, for the first time, that misfit dislocations in rippled, continuous InGaAs/GaAs layers are nucleated predominantly in the high stress regions at ripple troughs, as predicted previously [21,25]. The so-formed defect arrays conform to the ripple symmetry and spacing. This nucleation mechanism is likely to be of importance for all high-strain heteroepitaxial systems which exhibit surface nonplanarity (including SiGe/Si). The first defects observed to form in the present high misfit system appear to be faulted Frank partial dislocation half-loops. Dislocation reactions by which other common misfit defects (fault pairs and Lomer dislocations) can be formed have been given and, again, may be generally applicable to other epitaxial systems.

[1] F. C. Frank and J. H. van der Merwe, Proc. R. Soc. London A **198**, 205 (1949).

[2] F. C. Frank and J. H. van der Merwe, Proc. R. Soc. London A **201**, 261 (1949).

[3] W. A. Jesser and J. W. Matthews, Philos. Mag. **15**, 1097 (1967).

[4] W. A. Jesser and J. W. Matthews, Philos. Mag. **17**, 461 (1968).

[5] J. W. Matthews, S. Mader, and T. B. Light, J. Appl. Phys. **41**, 3800 (1970).

[6] J. W. Matthews and J. L. Crawford, Thin Solid Films **5**, 187 (1970).

[7] D. D. Perovic, G. C. Weatherly, J.-M. Baribeau, and D. C. Houghton, Thin Solid Films **183**, 141 (1989).

[8] D. J. Eaglesham, E. P. Kvam, D. M. Maher, C. J. Humphreys, and J. C. Bean, Philos. Mag. A **59**, 1059 (1989).

[9] K. Yagi, K. Takayanagi, K. Kobayashi, and G. Honjo, J. Cryst. Growth **9**, 84 (1971).

[10] C. Cherns and M. J. Stowell, Scr. Metall. **7**, 489 (1973).

[11] J. W. Matthews, J. Vac. Sci. Technol. **12**, 126 (1975).

[12] J. W. Matthews, A. E. Blakeslee, and S. Mader, Thin Solid Films **33**, 253 (1976).

[13] S. V. Kamat and J. P. Hirth, J. Appl. Phys. **67**, 6844 (1990).

[14] D. J. Eaglesham and M. Cerullo, Phys. Rev. Lett. **64**, 1943 (1990).

[15] C. W. Snyder, B. G. Orr, D. Kessler, and L. M. Sander, Phys. Rev. Lett. **66**, 3032 (1991).

[16] B. J. Spencer, P. W. Voorhees, and S. H. Davis, Phys. Rev. Lett. **67**, 3696 (1991).

[17] A. G. Cullis, D. J. Robbins, A. J. Pidduck, and P. W. Smith, in *Microscopy on Semiconducting Materials 1991*, edited by A. G. Cullis and N. J. Long (IOP Publishing Ltd., Bristol, 1991), p. 439.

[18] D. J. Robbins, A. G. Cullis, and A. J. Pidduck, J. Vac. Sci. Technol. B **9**, 2048 (1991).

[19] A. G. Cullis, D. J. Robbins, A. J. Pidduck, and P. W. Smith, J. Cryst. Growth **123**, 333 (1992).

[20] A. J. Pidduck, D. J. Robbins, A. G. Cullis, W. Y. Leong, and A. M. Pitt, Thin Solid Films **222**, 78 (1992).

[21] A. G. Cullis, D. J. Robbins, S. J. Barnett, and A. J. Pidduck, J. Vac. Sci. Technol. A **12**, 1924 (1994).

[22] J. Tersoff and F. K. LeGoues, Phys. Rev. Lett. **72**, 3570 (1994).

[23] D. J. Srolovitz, Acta Metall. **37**, 621 (1989).

[24] L. B. Freund, A. Bower, and J. C. Ramirez, Mater. Res. Soc. Symp. Proc. **130**, 139 (1989).

[25] D. E. Jesson, S. J. Pennycook, J.-M. Baribeau, and D. C. Houghton, Phys. Rev. Lett. **71**, 1744 (1993).

[26] A. G. Cullis, A. J. Pidduck, and M. T. Emeny, J. Cryst. Growth (to be published).

[27] P. R. Berger, K. Chang, P. Bhattacharya, J. Singh, and K. K. Bajaj, Appl. Phys. Lett. **53**, 684 (1988).

[28] E. A. Fitzgerald, Mater. Sci. Rep. **7**, 87 (1991).

[29] If the 220 diffraction geometry (with positive Bragg deviation) corresponding to images 2(c) and 2(d) is considered in terms of the scattering diagram shown in Fig. 10 of Ref. [19], with the sample upright under the electron beam, the lattice plane bending characteristic of stress relief in the ripple crests can be shown unambiguously to give bright or dark contrast with the specific symmetry in relation to the **g** vector seen for features 1–10.
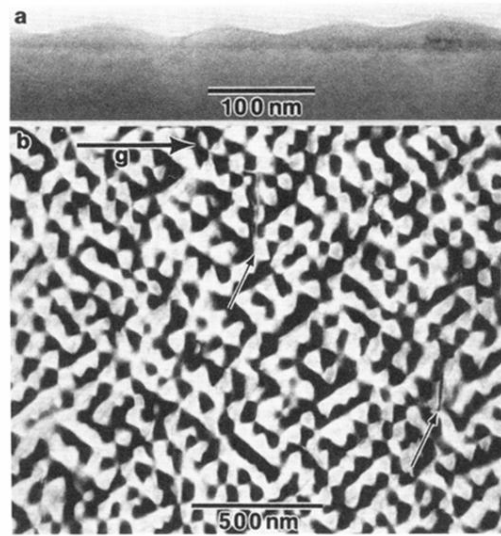
FIG. 1. (a) Cross-sectional [011] TEM image showing profile of surface ripples on $In_{0.25}Ga_{0.75}As$ epitaxial layer on GaAs, and (b) plan-view, strong-beam, $\mathbf{g} = 0\bar{2}2$, TEM image showing ordered ripple array and misfit defects (arrowed).
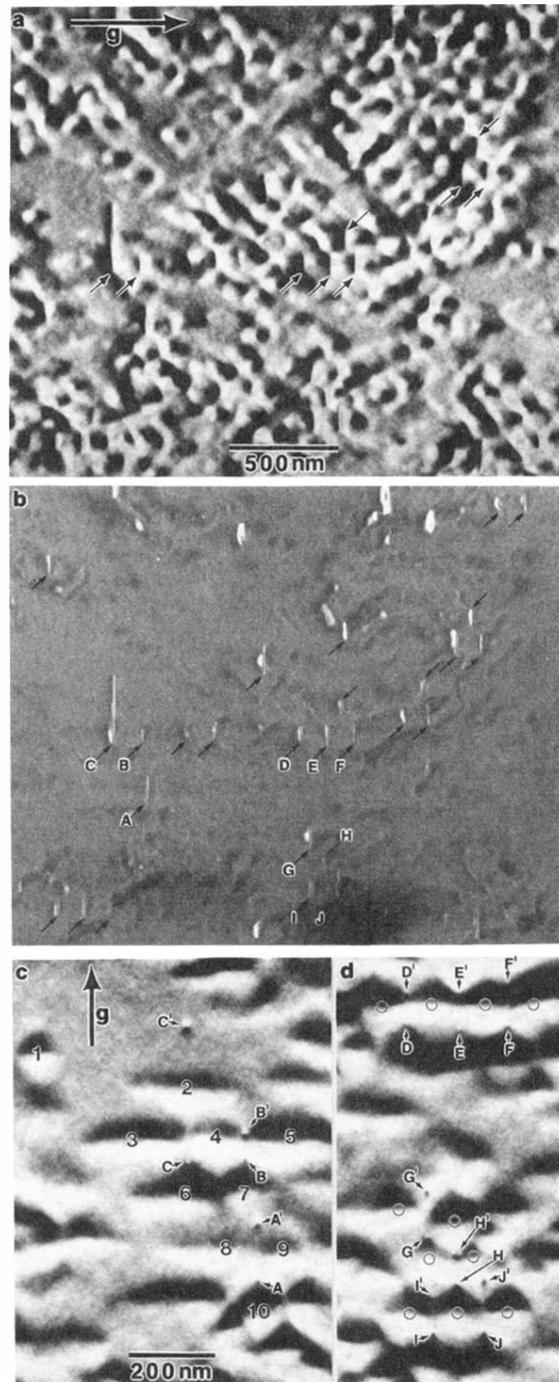
FIG. 2. Plan-view TEM images showing misfit defects among discontinuous ordered ripple arrays (a) strong-beam, $\mathbf{g} = 0\bar{2}2$, (Bragg deviation positive) with a selection of misfit defects arrowed; (b) weak-beam, dark-field $\mathbf{g} = 0\bar{2}2$ with misfit defects arrowed; (c),(d) strong-beam $\mathbf{g} = 022$ (Bragg deviation positive) showing misfit defect terminations A-A' to J-J' and selected surface ripple ridge sections numbered in (c) and marked with circles in (d).
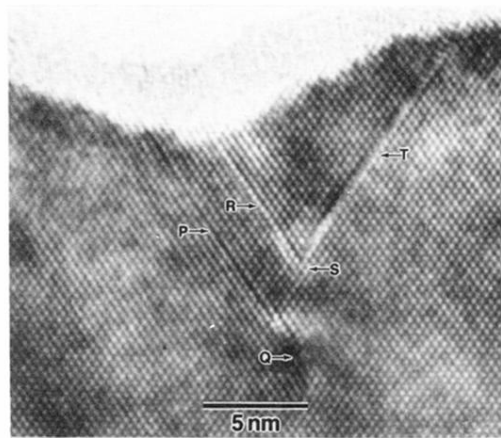
FIG. 3. Cross-sectional high resolution TEM image, [011] surface normal, showing misfit defects nucleated at surface ripple trough: stacking fault (*P*) bounded by Frank partial dislocation (*Q*, note terminating lattice fringe parallel to fault plane) and stacking fault (*R*) bounded by stair-rod dislocation (*S*) leading to secondary fault (*T*).